

Development of trains of ultrashort strain solitons in sapphire and ruby

Otto L. Muskens and Jaap I. Dijkhuis

Atom Optics and Ultrafast Dynamics, Debye Institute, University of Utrecht, P.O. Box 80 000, 3508 TA, Utrecht, The Netherlands;

ABSTRACT

Ultrashort strain pulses are a promising tool for the analysis and manipulation of condensed matter, thin films, and nanostructures. We present a new and unconventional way to generate coherent longitudinal acoustic wavepackets of high amplitude in the THz frequency range using the nonlinear development of picosecond strain pulses in a crystal. Our work [PRL 89, 285504 (2002)] demonstrated breakup of an initial wavepacket into a train of ultrashort strain solitons, using position-dependent Brillouin scattering. We extend in this paper the interpretation of the Brillouin scattering data in terms of optical Bragg reflections off the moving soliton train, using the analogy with an N -slit diffraction grating. Finally, we show that these short pulses can excite an electronic two-level system at THz resonance frequency, allowing for coherent amplification and even the development of a phonon laser.

Keywords: Terahertz, Phonon, Soliton, Brillouin-scattering

1. INTRODUCTION

Strain pulses of very short time duration are receiving considerable attention. As an extension of conventional ultrasonics in the nanometer size regime, the method of picosecond ultrasonics¹ has found wide application as an imaging tool in scientific and industrial environments. In combination with confocal microscopy or near field probing^{2,3} this would allow for a detailed study of the properties of small structures and their mechanical coupling to the environment.^{4,5} All generation methods for coherent strain wavepackets of picosecond time duration rely on ultrafast excitation of a thin-film transducer using optical pulses from a femtosecond laser. For application as a transducer material, metal films are very suitable by their short optical absorption length. Acoustic strain wavepackets in metal films are ultimately limited in width by this skin depth to frequencies of several hundred GHz.^{1,6} However, the finite electronic mean free path and heat diffusion during the first moments after excitation^{7,8} limit generation of high-frequency components to only the thinnest of metallic films.

The research of acoustic pulse formation in semiconductor materials is relatively recent and unexplored. Ultrafast excitation of quantum wells and multilayer structures has nevertheless demonstrated the formation of localized (ZFLAP) and extended coherent acoustic vibrations at THz frequencies.⁹⁻¹² The utilization of epitaxially grown structures for THz phonon generation is certainly advantageous to prevent diffusive boundary scattering of high-frequency phonons from surface irregularities.

A new and challenging avenue has only recently be explored, that deals with the propagation of picosecond strain wavepackets over macroscopic distances in bulk materials. It was found that, over these long travelling paths, the dispersion of the crystalline structure distorts the initial pulse shape by pulling apart the higher- and lower-frequency components.^{13,14} At larger initial amplitude of the strain packets, yet another property of the propagating medium appears.^{15,16} The anharmonicity of the interatomic potential results in a strain-dependent propagation velocity, causing shock fronts to occur in both phases of the bipolar wavepacket. The combination of phonon dispersion and lattice anharmonicity sets up a medium in which stable solitary waves are formed, that can propagate without distortion over macroscopic distances. The first publications on the topic of strain solitons have focused on the material properties that are responsible for the development of these stable nonlinear structures. In the future, however, one may expect application of these short pulses in other fields of materials

Further author information: (Send correspondence to Jaap I. Dijkhuis)

Jaap I. Dijkhuis: E-mail: J.I.Dijkhuis@phys.uu.nl, Telephone: +31 (0)30 253 23 19

science. Many typical properties of condensed matter and semiconductor materials, like electronic structure, phase behavior, and optical properties, have been shown to depend on applied pressure. The response of these materials to high-amplitude dynamic strains may reveal totally new phenomena on the ultrafast time scale. Interaction of these ultrashort strain packets with electronic two-level systems has already revealed completely novel time-dependent behavior.¹⁷ Further, coherent strain packets of very short time duration may be applied in surface science for imaging or even patterning of nanometer sized objects. The short acoustic wavelength of several nanometers sets a limit to the spatial resolution that can otherwise only be achieved in the x-ray range of the electromagnetic spectrum. The high strain amplitudes of the typical strain solitons is associated with a considerable amount of energy of $\sim 1 \mu\text{J}/\text{cm}^2$. The fact that this is contained within a temporal width of less than 0.5 ps may enable excitation via higher order nonlinear processes. Interaction of ultrashort strain pulses with excitons in quantum wells or superconducting thin-films is possible without depositing residual heat in the system, as the thermoelastic strain generation is well-separated from the studied structures by the bulk substrate. These are only a few directions of research that are possible with the ultrashort strain pulses presented in this paper.

2. THEORY OF STRAIN SOLITONS

In this section we summarize some concepts of nonlinear elasticity that found the theory of strain solitons. The multidimensional formulation of finite strain lattice dynamics reduces to the well-known Korteweg-de Vries (KdV) equation in one dimension for moderate strains. Solution of the KdV initial value problem leads to the development of trains of solitons.

2.1. Derivation of the KdV-equation

We follow the derivation and definitions as presented in the review of Wallace.¹⁸ The finite elasticity theory is derived starting from the change in length $(\Delta s)^2$ of a local vector in the material under deformation. The position dependent deformation can be captured by a tensor equation $(\Delta s)^2 = \eta_{ij} \Delta r_i \Delta r_j$, where r_i are the curvilinear coordinates in the material. In this expression, the strain η_{ij} follows as

$$\eta_{ij} = \frac{1}{2}(u_{ij} + u_{ji} + u_{ik}u_{kj}) , \quad (1)$$

where

$$u_{ij} = \frac{\partial u_i}{\partial r_j} \quad (2)$$

describes the displacement gradient matrix elements. Now, having an expression for the deformation at all positions in the material, it will be necessary to estimate the amount of free energy involved in this deviation from the equilibrium state. One can only obtain such an estimate when the internal energy Φ per unit of mass ρ is known as a function of strain in the form

$$\rho\Phi_S(\vec{r}, \eta) = \rho\Phi_0 + C_{ij}\eta_{ij} + \frac{1}{2}C_{ijkl}\eta_{ij}\eta_{kl} + \frac{1}{6}C_{ijklmn}\eta_{ij}\eta_{kl}\eta_{mn} + \dots \quad (3)$$

Here the subscript S denotes that the deformation occurs at constant entropy, i.e. under adiabatic conditions. The constants C are the elasticity constants of first, second and third order, respectively defined by the first- and higher-order partial derivatives of the internal energy to the strain elements, $C_{ij} = \partial\Phi_S/\partial\eta_{ij}$, $C_{ijkl} = \partial^2\Phi_S/\partial\eta_{ij}\partial\eta_{kl}$, etc. These constants have been determined experimentally for a large number of materials.

When the change in free energy is expressed as a function of applied strain, the Lagrangian density can be written as the difference of kinetic and potential energy as

$$L = \frac{1}{2}\rho\dot{r}'_i\dot{r}'_i - \rho\Phi_S(\vec{r}, t). \quad (4)$$

The equations of motions for the independent components r'_i are now formulated using the Euler-Lagrange equation

$$\frac{\partial}{\partial t} \frac{\partial L}{\partial \dot{r}'_i} + \frac{\partial}{\partial r_k} \frac{\partial L}{\partial \alpha_{ik}} = 0, \quad (5)$$

with the abbreviation $\alpha_{ik} = \partial r'_i / \partial r_k$.

After some rearrangement and maintaining terms only to the third order of the displacement derivatives, one obtains the general expression for the nonlinear wave equation¹⁸

$$\rho \ddot{u}_i = \frac{\partial u_{jk}}{\partial r_l} (C_{ijkl} + u_{pq} A_{ijklpq}). \quad (6)$$

It should be noted that the term A_{ijklmn} contains a combination of third-order *and* second order elastic constants:

$$A_{ijklpq} = C_{jlpq} \delta_{ik} + C_{ijql} \delta_{kp} + C_{jkql} \delta_{ip} + C_{ijklpq}. \quad (7)$$

The second-order coefficients in this expression are a consequence of the presence of the quadratic term in the definition of strain, Eq. (1). Therefore, these contributions to the nonlinear term in the propagation equation, Eq. (6), are sometimes referred to as the *geometrical* nonlinearity, whereas the third order constants are called the *physical* nonlinearity. One may convert the elastic constants in Eq. (6) and (7) to tabulated values in Voigt notation by the reduction of pairs of indices according to $11 \rightarrow 1, 22 \rightarrow 2$, etc.

In the case of one-dimensional propagation along an axis of high symmetry z , the equation of motion, Eq. (6), reduces to the simple form

$$\rho u_{tt} = \gamma u_{zz} + \alpha u_z u_{zz}, \quad (8)$$

where the subscripts denote differentiation. The last term on the right side is the quadratic nonlinearity, due to the geometric nonlinearity and the cubic terms in the inter-atomic potential. The nonlinearity coefficient α depends only on the propagation direction in the crystal. For the [0001]-direction in a trigonal crystal like sapphire the two constants of Eq. (8) take on the form [c.f. Eq. (7)]

$$\gamma = C_{33}, \quad \alpha = (3C_{33} + C_{333}), \quad (9)$$

where the coefficients C_{33} and C_{333} are the second- and third-order elastic moduli in the [0001]-direction. For most solids, the contribution of the third order modulus is larger than the geometric term and has a negative sign, yielding an $\alpha < 0$.

Up to this point, we have not taken into account any dispersion in the equation of motion. In the case of longitudinal acoustic lattice vibrations (LA phonons) in a crystalline solid, the dispersion due to discreteness of the lattice can be written as¹⁹

$$\omega = \sqrt{\frac{4C_{33}}{M}} \sin |ka/2|. \quad (10)$$

As we will be dealing with vibrations of small wavevector, i.e. in the center of the Brillouin zone, it is sufficient to approximate this dispersion relation by its first two nonzero expansion terms

$$\begin{aligned} \omega &= c_0 k - \beta k^3, \\ \beta &= \frac{c_0^3}{6\omega_{max}^2}, \end{aligned} \quad (11)$$

where ω_{max} is the LA angular frequency at the edge of the Brillouin zone. This dispersive correction can be put into Eq. (8), leading to a fourth-order spatial derivative (see e.g. Ref [15]). At this point it is further convenient to switch from the displacement coordinate u to an uniaxial component of the acoustic strain, further denoted as s . This is done by differentiation of Eq. (8) with respect to the z -coordinate. Given the initial wave packet at $t = 0$ of amplitude s_0 and shape $\phi(z)$, the resulting boundary value problem including dispersion, reads

$$\begin{aligned} s_{tt} - c_0^2 s_{zz} - \frac{\alpha}{\rho} \frac{\partial}{\partial z} (s s_z) - 2c_0 \beta s_{zzzz} &= 0, \\ s(z, t = 0) &= s_0 \phi(z). \end{aligned} \quad (12)$$

Finally it is convenient to transform to a moving frame coordinate system, defined by the parameters $t' = t$, $y = z - c_0 t$. After substitution of these variables we arrive at terms consisting of only one derivative with respect

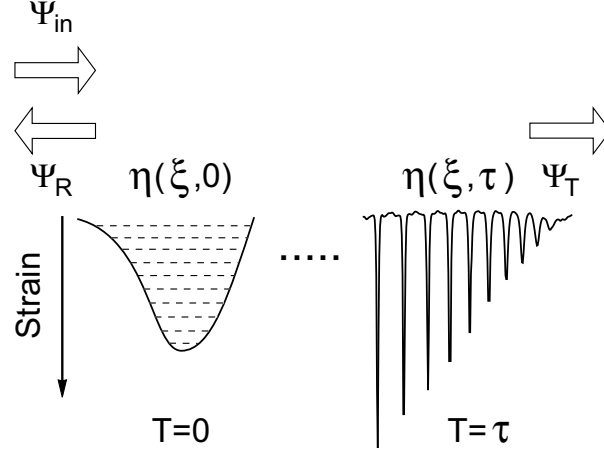


Figure 1. Visualization of inverse scattering method, where the time development of the wavepacket is mapped onto an eigenvalue problem for a time varying potential $\eta(\xi, \tau)$. The evolution at large times can be recovered from the reflected and transmitted wavefunctions Ψ_R, Ψ_T .

to the travelling coordinate y , except for one term having a double time derivative $s_{t't'}$. Neglecting this term will not change the behavior up to first order,²⁰ as this is a 'slow' coordinate with respect to the evolution of the wave packet. Integrating the resulting expression once, we finally obtain the equation

$$\begin{aligned} s_{t'} + \frac{\alpha}{2\rho c_0} s s_y + \beta s_{y y y} &= 0 \\ s(y, t' = 0) &= s_0 \phi(y) . \end{aligned} \quad (13)$$

This is the well-known Korteweg-de Vries (KdV) equation, describing for example the formation of stable wave packets (solitons) in a narrow water channel.²¹ It can be shown that solutions of Eq. (13) also fulfill its spatial derivative, although the reverse is not necessarily true. In the experimental configuration in the sapphire crystal, $\alpha < 0$ and $\beta > 0$, resulting in soliton development for $s < 0$, i.e. for compressional strain pulses.

2.2. Analytical solutions

We are interested in the development of an initial waveform $s(z, t) = s_0 \phi(z/l_0)$, where s_0 and l_0 are the typical amplitude and width of the strain packet. After transformation to the coordinates $\eta = s/s_0$, $\xi = z/l_0$, and $\tau = t\alpha s_0/2\rho c_0 l_0$, the initial value problem of Eq. (13) takes on the form²⁰

$$\begin{aligned} \eta_\tau + \eta \eta_\xi + \frac{1}{\sigma^2} \eta_{\xi \xi \xi} &= 0 \\ \eta(\xi, 0) &= \phi(\xi), \end{aligned} \quad (14)$$

where σ is a dimensionless parameter defined by

$$\sigma = l_0 \left(\frac{\alpha s_0}{2\rho c_0 \beta} \right)^{1/2} . \quad (15)$$

Equation (14) yields identical solutions for initial wavepackets with the same value of σ and $\phi(\xi)$, and therefore σ is called the similarity parameter. The magnitude of σ measures the relation between nonlinearity and dispersion in the wavepacket development. Note that σ is proportional to the area under the square root of the strain waveform.

For the KdV-initial value problem Eq. (14) there exists an associated eigenvalue problem for the Schrödinger equation²²

$$\Psi_{\xi\xi} + \frac{\sigma^2}{6} (\lambda - \eta(\xi, \tau)) \Psi = 0. \quad (16)$$

In a normal scattering problem, one is interested in the eigenvalues and reflection and transmission functions for a given potential $\eta(\xi, \tau)$. The inverse scattering problem amounts to the reconstruction of the potential for a set of known scattering quantities, i.e. energy levels, reflection and transmission functions [see Fig. 1]. The solutions of this eigenvalue equation can consist of free or bound states, depending on the sign of the initial potential $\phi(\xi)$. The reflection and transmission coefficients can be derived using the time dependence of the eigenfunctions Ψ , as follows from the KdV equation for the potential $\eta(\xi, \tau)$. This evolution can be determined by writing $\eta(\xi, \tau)$ in terms of Ψ using Eq. (16) and substituting it into the KdV equation, Eq. (14). A concise overview of the inverse scattering method for the KdV-initial value problem can be found in Refs. [20, 23]. We limit our discussion to the most important results for this paper, namely the resulting expressions for the potential energy for a discrete spectrum of eigenmodes $\lambda_n < 0$. It turns out that all bound states of the initial potential $\phi(\xi)$ correspond to soliton-pulses of the form

$$\eta(\xi, \tau) = -12k_n^2 \text{sech}^2(k_n(\xi - \xi_0) - 4k_n^3 t), \quad (17)$$

where $k_n = \sqrt{-\lambda_n/6} > 0$. From this expression it can be observed that the amplitude of the n -th soliton is $\eta_n = 2\lambda_n$, or $a_n = 2\lambda_n s_0$ in normal strain units. The velocity of these solitons is $\partial\xi/\partial\tau = \eta_n/3$ in normalized coordinates, or $c_n = \alpha a_n/6\rho c_0$ in real coordinates [c.f. Eq. (14)].

An analytical solution of the eigenvalue equation, Eq. (16) may be obtained in several special cases of the initial waveform $\phi(\xi)$. In particular, the spectrum of eigenvalues for a potential of the form $\phi(\xi) = \text{sech}^2\xi$ can be obtained in the analytical form²⁴

$$\frac{a_n}{s_0} = \frac{3}{\sigma^2} \left(1 - 2n + \sqrt{1 + 2\sigma^2/3}\right)^2 \quad (18)$$

However, in our experiments we will be dealing with strain pulses that have a profile given to good approximation by the derivative of a Gaussian. Thus we want to relate the estimate of Eq. (18) to the initial condition

$$s(y, 0) = \frac{\sqrt{2}\sqrt{e}}{l_g} s_0 y \exp(-y^2/l_g^2), \quad (19)$$

that is normalized to s_0 at its maximum at $y = l_g/\sqrt{2}$. In order to rescale to the dimensionless form $\phi(\xi)$, we normalize the integrals of the square root of the waveform Eq. (19) and that of the sech^2 -waveform. This amounts to the redefinition of the pulse width as $l_0 = e^{1/4}\Gamma(3/4)l_g/\pi$, with l_0 the width of the pulse in the sech^2 -waveform (Γ denotes the Euler gamma-function). By replacing this length scale in Eq. (19), normalizing to s_0 , and transforming to $\xi = y/l_0$ we obtain the dimensionless initial waveform $\phi(\xi)$, and the associated σ for calculation of the number of solitons in Eq. (18).

2.3. Transition from shock waves to soliton trains

In reality, at all but the lowest temperatures, acoustic waves will be attenuated by scattering via thermal phonons under propagation through a crystal. Classically, this can be accounted for by including an additional viscosity term in the wave equation²⁵

$$\begin{aligned} s_t + \frac{\alpha}{2\rho c_0} s s_y - \epsilon s_{yy} + \beta s_{yyy} &= 0 \\ s(y, t' = 0) &= s_0 \phi(y) . \end{aligned} \quad (20)$$

This combination of nonlinearity, dispersion, and viscosity in the wave equation is called the Korteweg-de Vries-Burgers (KdV-Burgers) equation. Unlike the KdV-initial value problem, this is not an integrable equation and solution can only be obtained numerically. For special situations, however, we may neglect either one of the three constituent terms and recover either the KdV-, the Burgers- or a linear wave equation. In most situations where all terms are relevant, we have to rely on the numerical simulations of the KdV-Burgers equation presented in the next section.

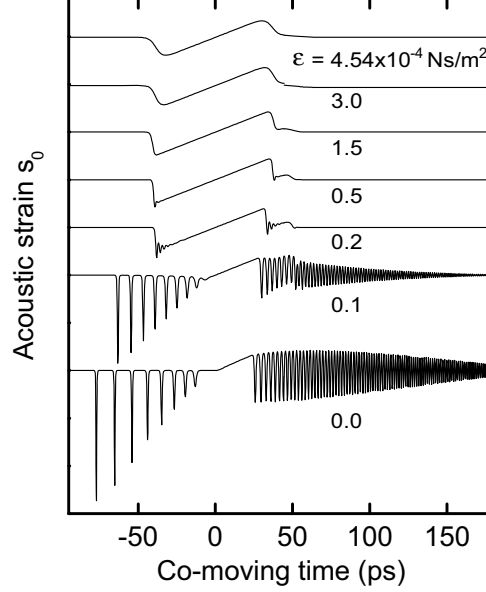


Figure 2. Time-domain traces at $z = 1$ mm of the simulated acoustic wavepacket for different values of the viscosity ϵ . Results are obtained using the KdV-Burgers equation at an initial strain $s_0 = 1.4 \times 10^{-3}$, using the finite volume method of Eq. (21).

2.4. Numerical simulations

Constructing a numerical solution for a nonlinear, dispersive wave equation with initial conditions is a specialized topic in itself. The combination of a large nonlinear and small dispersive term that occurs in our experimental configuration demands a high level of stability and efficiency of the algorithm. As an example, the simulation of soliton train development over ~ 1 cm propagation distance in sapphire requires a co-moving time array of around 10^6 points, and over 10^5 iteration steps to obtain stable solutions. In these extreme conditions, it is important that the scheme is fast, for example, the amount of computational effort between N^2 and N^3 operations is of order $N \approx 10^6$ for the above example. This already eliminates the most simple of PDE solving methods, namely that of brute-force inversion of the finite difference matrix (which is an N^3 -process). In the course of this work we have attempted three different implementations of nonlinear PDE-solving routines, two of them based on fast Fourier transforms (FFT)^{26,27} and one using finite difference techniques.²⁸ Of these, only two were stable enough at the high mesh sizes and nonlinearity under study to perform simulations. The leapfrog method of Ref. [26], due to its intrinsic unstableness,^{29,30} turned out inappropriate for our current problem.

We show here the finite volume discretization^{28,29} for the KdV-Burgers equation as used in our simulations. Spatial derivatives are calculated using the common discretization at the highest time level. Note that an integration has taken place around the grid points i , therefore the evaluation takes place at positions $w = (s_i + s_{i-1})/2$ and $e = (s_{i+1} - s_i)/2$,²⁹ resulting in the difference equation

$$h \frac{3s^{n+1} - 4s^n + s^{n-1}}{k} - \epsilon \frac{s_{i+1}^{n+1} - 2s_i^{n+1} + s_{i-1}^{n+1}}{h} + \beta \frac{s_{i+2}^{n+1} - 2s_{i+1}^{n+1} + 2s_{i-1}^{n+1} - s_{i-2}^{n+1}}{2h^2} + \frac{\alpha}{2\rho c_0} \left(\frac{1}{8}(s_{i+1}^{n+1} + s_i^{n+1})(s_{i+1}^n + s_i^n) - \frac{1}{8}(s_i^{n+1} + s_{i-1}^{n+1})(s_i^n + s_{i-1}^n) \right) = 0. \quad (21)$$

This equation can be easily rewritten in the form of a vector equation $L(\vec{S}^n)S^{n+1} = b\vec{S}^n + c\vec{S}^{n-1}$, where \vec{S} denotes the spatial grid of strain values, and $L(\vec{S}^n)$ is a band diagonal matrix containing both the linear and nonlinear finite difference terms. The initial conditions have to be applied via two initial state vectors, $\vec{S}^{n=0}$ and $\vec{S}^{n=1}$. The latter may be estimated using a simple Euler-forward iteration, or with small enough time steps the simulation starts up when $\vec{S}^{n=1} = \vec{S}^{n=0}$. The solution of the matrix equation can be done efficiently using

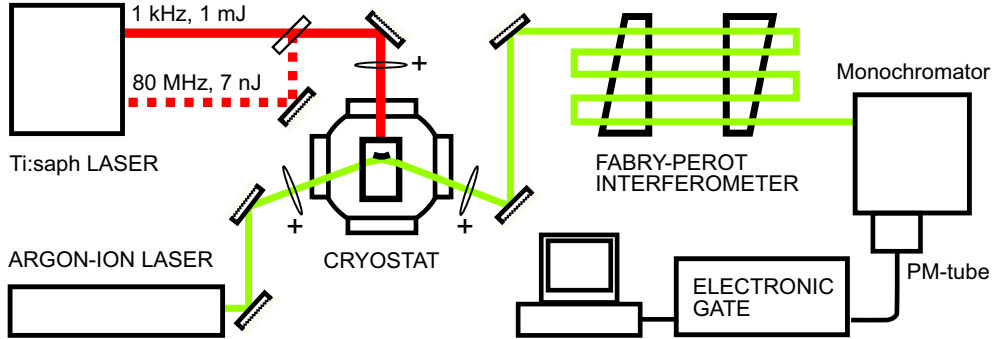


Figure 3. Brillouin scattering setup, showing pump and brillouin scattering laser, optical cryostat and detection setup.

standard inversion algorithms for sparse matrices,³¹ that use order N^2M operations, with N the number of points in the mesh and M the width of the band in the matrix ($M = 5$ in our system).

3. EXPERIMENTAL SETUP

For the propagation experiments we use a piece of high-quality (< 1 ppm. impurity ions) single-crystal sapphire of $5 \times 11 \times 10$ -mm³ dimensions, with the c -axis aligned perpendicular to the 5×11 -mm² surface, that is covered with a 100-nm thin chromium transducer. The crystal is mounted into an optical cryostat to perform experiments down to liquid helium temperatures. Strain wavepackets of very short (picosecond) time duration are generated using the conventional method of ultrafast heating of the chromium film that is evaporated onto the sapphire substrate. It is well known that chromium has a very high electron-phonon coupling constant of $\sim 420 \times 10^{15}$ W/m³ K, and thus the electronic excitation is converted to a coherent strain over a distance of the order of the optical absorption length.^{7,32} Acoustic strain pulses in the high-amplitude regime are generated using an amplified Ti:sapphire laser setup, which provides 130-fs laser pulses at 800 nm with an energy of ~ 0.75 mJ/pulse, at a repetition rate of 1.0 kHz.¹⁶ To obtain excitation over a large area, the output of this laser is weakly focused to a spot of loosely several millimeters in diameter onto the sample. The optical pump fluence is varied by controlling the position of this focusing lens, the upper limit being the damage threshold of our transducer at ~ 15 mJ/cm². Small-area, low-amplitude acoustic pulses can be generated as well, using the mode-locked output of the system, carrying 7 nJ/pulse at a repetition rate of 80 MHz.

4. BRILLOUIN SCATTERING

For the detection of acoustic strain we make use of the Brillouin-scattering technique. In contrast to time-domain pump and probe-methods, which are inherently sensitive only at a reflecting interface, inelastic light scattering enables detection of strain components in the *bulk* of a transparent crystal. Conservation of energy and momentum in the scattering process implies sensitivity to individual Fourier-components of the acoustic wave packet.³³ Figure 3 shows the experimental configuration for the scattering experiment. The optical probe is a single-mode argon-ion laser operating at 514.5 nm and delivering 60 mW optical output power. The optical beam is tightly focused inside the crystal to a waist of several micrometers. The frequency-shifted scattered radiation is analyzed by a quintuple-pass Fabry-Perot interferometer (Burleigh RC110) and detected using standard photon counting techniques. The spectrometer has been used earlier to study the propagation of coherent, monochromatic phonon beams in lead molybdate and paratellurite.³⁴⁻³⁶

4.1. Polarization dependence

It is well-known that the elasto-optic coupling efficiency in sapphire shows a strong anisotropy for electromagnetic waves propagating perpendicular to the c -axis.^{37,38} Therefore we have determined the dependence of the Brillouin scattering efficiency on the polarization angle of the probe-laser beam (see Fig. 4). We use excitation by the 80-MHz, modelocked Ti:sapphire laser that allows for a dynamic range of about 10^4 in intensity. Indeed, a very strong variation over three orders of magnitude of the scattered intensity as a function of probe-beam

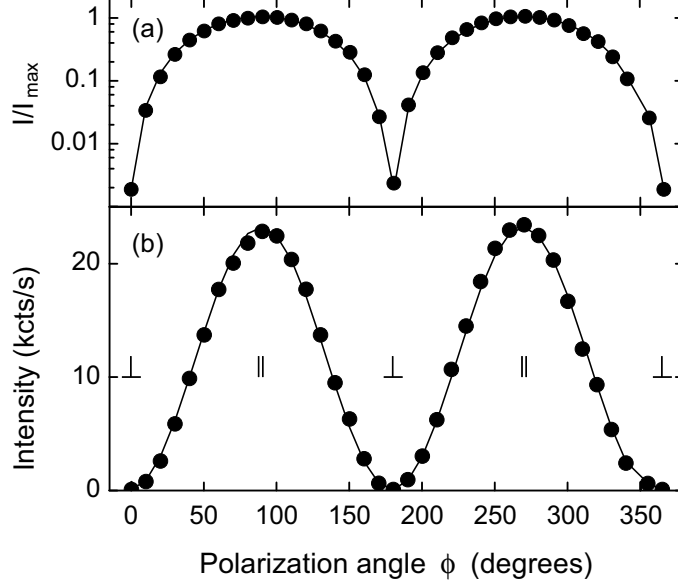


Figure 4. Dependence of Brillouin scattering signal at a frequency of 22 GHz on argon-ion laser polarization, (a) Logarithmic, normalized to maximum and (b) linear scale. (\parallel , \perp) indicate orientation of electric-field vector \vec{E} to the crystallographic c -axis

polarization angle ϕ is observed, that can be explained by the sum of the electric-field components parallel and perpendicular to the c -axis:

$$I(\phi) = a (p_{33}^2 \sin^2 \phi + p_{13}^2 \cos^2 \phi), \quad (22)$$

where p_{33}, p_{13} denote the elasto-optic coupling parameters for $\vec{E} \parallel c$ and $\vec{E} \perp c$, respectively, and a is an arbitrary scaling factor. The observed ratio $p_{33}/p_{13} \approx 22$, which is somewhat smaller than expected from literature, where $p_{33} = 0.23, p_{13} \leq 0.005$.³⁷ This difference will be most likely due to the angle of incidence of the probe beam of about 20° , which results in some mixing with the elasto-optic component $p_{31} \approx 0.03$. Without going into further detail on this, we have chosen to maximize the Brillouin scattering intensity, using the $\vec{E} \parallel c$ polarization.

4.2. Strain calibration

We can gauge the Brillouin spectrum induced by the coherent strain packet to the thermal phonon background of ~ 40 cts/s, measured in sapphire at 22 GHz at room temperature. As the scattered intensity scales with the occupation number of the phonons under study, we obtain an estimate for the occupation of the coherent packet of $n_\omega \approx 10^3 n_{\text{th}}$, or an apparent mode temperature exceeding 10^5 K, for excitation using a modelocked laser at a fluence of ~ 0.5 mJ/cm² per pulse. It is well known that for a harmonic oscillator, the average energy is equally distributed over the potential and kinetic parts, $U = T = \frac{1}{2} \hbar \omega (n_\omega + \frac{1}{2})$. Combined with the expression for the potential energy $U = \frac{1}{2} M \omega^2 |\bar{u}_\omega|^2$, and the number of oscillators given by the Debye density of states $D(\omega) \Delta \omega$, we obtain the expression for the average wave amplitude of the spectral component \bar{u}_ω , given by

$$\bar{u}_\omega = \left(D(\omega) \Delta \omega \frac{(n_\omega + \frac{1}{2}) \hbar}{M \omega} \right)^{1/2}. \quad (23)$$

As we are dealing with a very directional beam of phonons, the complete, 3-dimensional density of states will hugely overestimate the number of participating oscillators. We therefore take into account only a cone of wavevectors, with a top angle defined by the acceptance angle of the detector, $\theta_0 \approx 50$ mrad. Integration over only this part of phase space yields a more realistic density of states $D(\omega) \Delta \omega \approx V \omega^2 \theta_0^2 \Delta \omega / 4\pi c_0^3$.

From Eq. (23) we can obtain the associated strain $\bar{s}_\omega = \partial \bar{u}_\omega / \partial x$ by multiplication with ω/c_0 . For our example at 22 GHz, this results in a displacement of $\bar{u}_\omega = 3 \times 10^{-14}$ m, or an acoustic strain $\bar{s}_\omega = 3.5 \times 10^{-7}$, over a

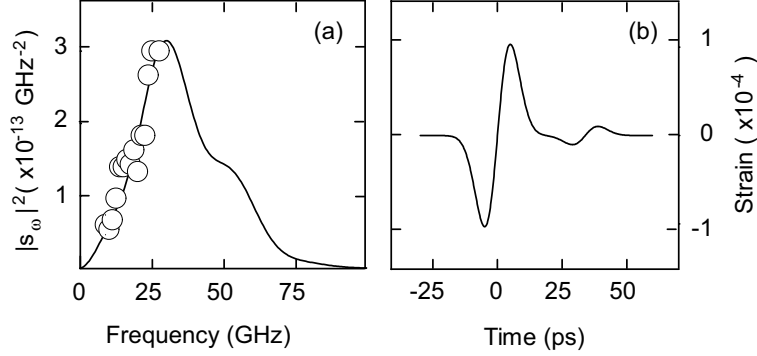


Figure 5. Power spectrum (a) and time-domain waveform (a) of simulated acoustic wavepackets in sapphire. (o) are experimental data from Brillouin scattering. Vertical scale of (a) is calibrated scale against thermal phonon background at 22 GHz, scale (b) is strain amplitude corresponding to calibrated spectrum.

finesse-limited bandwidth of 0.8 GHz (at a free spectral range of 42 GHz). We can even go further and gauge the overall spectrum of Fig. 5(a) to this value. The calibrated scale for the power density $|\bar{s}_\omega|^2$ is shown on the left side of this graph. The inverse Fourier transform of this calibrated spectrum, finally, results in an estimate of the coherent strain amplitude of 10^{-4} for the ‘modelocked’ wavepackets.

In the case of excitation by amplified laser pulses, we measured a maximum intensity of the order of 1 kcts/s at $E = 8 \text{ mJ/cm}^2$ pump fluence. Accounting for the reduction in repetition rate of 8×10^4 , this yields a $\bar{u}_\omega = 2.1 \times 10^{-12} \text{ m}$, corresponding to a coherent strain amplitude of 4×10^{-3} .

5. SOLITON TRAINS AND BRAGG GRATINGS

Figure 6 shows a typical trace of the Brillouin intensity as a function of the travelled distance in the crystal, at $E = 5 \text{ mJ/cm}^2$. Similar traces were presented in Ref. [16] and explained using the numerical simulations of the KdV equations. We can attribute the initial strong decay of the scattered intensity to the self-steepening of the initial wavepacket, leading to a shock front at both sides of the pulse [c.f. Fig 2] and N-wave formation. This process is accompanied with a redistribution of spectral components from the initial small band below 100 GHz [see Fig. 5(a)] to a range of frequencies as high as 1 THz. The following oscillations were attributed to spatial resonances and Bragg-reflection from the light scattered from the strain solitons moving at different velocities.

At this point we draw our earlier interpretation in terms of Bragg scattering from moving solitons a little further by considering the analogy between the soliton train and a diffraction grating. Let us consider a train of δ -functions given by

$$f(z, t) = \sum_{j=1}^N a_j \delta(t + \gamma_j z), \quad (24)$$

with N the number of solitons, a_j the soliton amplitudes, and $\gamma_j = v_j/c_0^2$ the soliton walkoff in the moving frame system. Unfortunately, for the real soliton train as defined by the amplitudes of Eq. (18), there is no periodicity and thus Eq. (24) does not reduce to a simple form. However, we may approximate the expression for the first few solitons in the train, at large values of σ , by the linear expansion

$$a_j \approx 2s_0 \left(1 - 4\sqrt{6}j/\sigma\right). \quad (25)$$

For the equidistant train of Eq. (25), $\gamma_j = j\Delta\gamma$ and $a_j = j\Delta a$, with $\Delta a = 8\sqrt{6}s_0/\sigma$ the amplitude difference and $\Delta\gamma = 4\sqrt{6}\alpha s_0/3\sigma\rho c_0^3$ the walkoff between subsequent solitons [c.f. Eq (17)]. In this case, it is useful to consider the train f of Eq. (24) as a product of a comb-function g with a triangular shape h :

$$f(z, t) = g(z, t) \cdot h(z, t) \quad (26)$$

$$g(z, t) = \sum_{j=1}^N \delta(t + j\Delta\gamma z), \quad h(z, t) = \frac{\Delta a}{\Delta\gamma z} t. \quad (27)$$

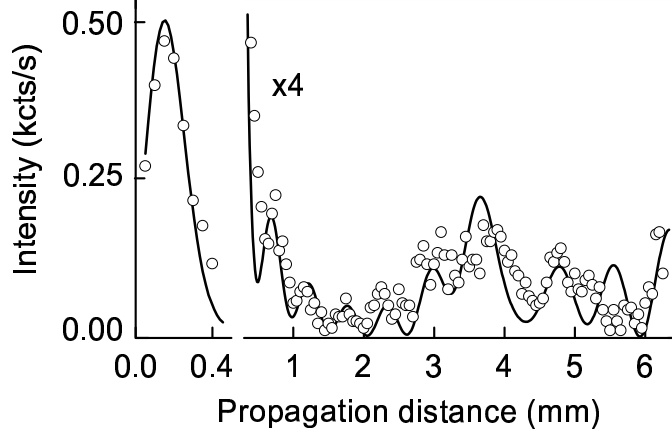


Figure 6. Dependence of Brillouin scattering signal at a frequency of 22 GHz on propagation distance z in the crystal. (○) experimental data, (line) numerical simulation using KdV equation.

After fourier transformation, this product will be transformed into the convolution $\tilde{f} = \tilde{g} \otimes \tilde{h}$, with \tilde{g} and \tilde{h} the transforms of the comb and triangular functions, respectively given by

$$\tilde{g}(z, \omega) = (2\pi)^{-1/2} \frac{\sin N\beta\omega}{\sin \beta\omega} e^{-i\beta\omega(N+1)}, \quad (28)$$

$$\tilde{h}(z, \omega) = -i\zeta \frac{\partial}{\partial \omega} \delta(\omega), \quad (29)$$

with the abbreviations $\beta = \Delta\gamma z/2$ and $\zeta = (2\pi)^{1/2} \Delta a/\Delta\gamma z$. The above expression for \tilde{g} is the well-known transform function for a grating with N slits, indicating that the frequency spectrum of the equidistant soliton train can be interpreted in terms of the diffraction orders of a grating. For completeness, we give the exact solution of the above convolution equation. Partial integration yields

$$\begin{aligned} \tilde{f}(z, \omega) &= -i\zeta \left. \frac{\partial}{\partial \omega'} \tilde{g}(\omega - \omega') \right|_{\omega'=0} \\ &= \zeta \beta \tilde{g}(\omega) \left(N + 1 + iN \frac{\cos(N\beta\omega)}{\sin(N\beta\omega)} - i \frac{\cos(\beta\omega)}{\sin(\beta\omega)} \right). \end{aligned} \quad (30)$$

The power spectrum corresponding to this expression can be observed as the dotted line in Fig. 7(c). The overall periodicity in this equation is determined by the zeros of the denominator of \tilde{g} , with spacing $\Delta\omega_0/2\pi = 1/2\beta \approx 102.5$ GHz. Further it turns out that there are exactly $(N - 1)$ subminima between the main orders, with a period $\Delta\omega_1 = \Delta\omega_0/N$, although their visibility is reduced by the additional terms in Eq. (30).

We can now understand the shape and periodicity of the spectrum in Fig. 7(c) by the grating properties of the equidistant soliton train. It is even possible to determine the number of solitons from the fine structure in the spectrum, by counting the oscillations between the main grating orders. If we now compare the simple form of Fig. 7(c) with the spectrum of Fig. 7(b), it is clear that the variations in spacing in the real soliton train are sufficient to destroy the periodicity of the grating function. Still, however, the part of the spectrum below, say 100 GHz, seems to correspond reasonably well to the pattern observed in the equidistant soliton train below the first grating order. The bump around 135 GHz may even be attributed to constructive interference of the slightly smaller spacings in the realistic train of Fig. 7(a). Thus, by counting the number of oscillations before this maximum, we may get an impression, or lower limit, of the number of solitons in the train. For example, in Fig. 7(b) we can count up to 7 minima before the first order maximum at 135 GHz, giving an estimate of $N = 8$. This means that we underestimate the number of solitons by only two or three. The unaccounted solitons are probably the numbers 6,8 and 10 in the train of Fig. 7(a), that are positioned between the peaks of the equidistant train and thus are the least resonant with the first few solitons in the grating.

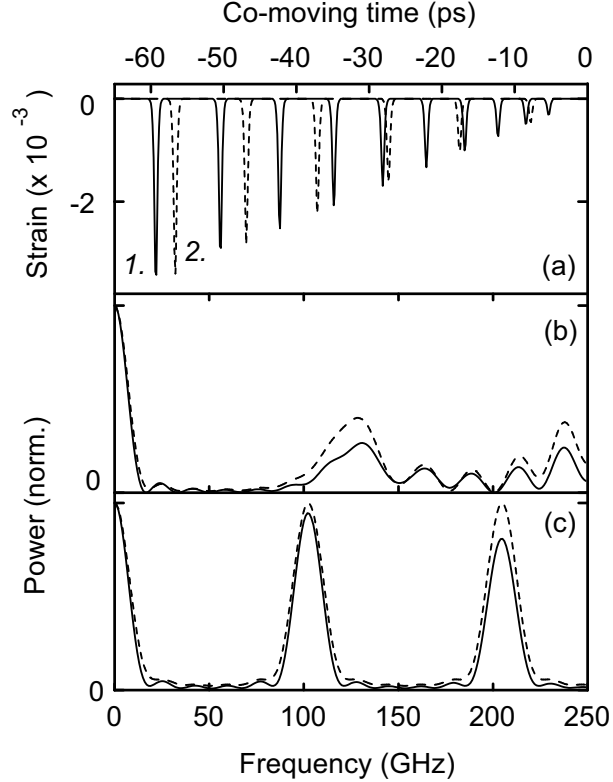


Figure 7. (a) Analytical soliton trains after 0.5 mm, using 1. real form, Eq. (18) (solid) and 2. equidistant approximation, Eq. (25) (dash). (b) Power spectrum of the train 1. of (a) (solid), and (dash) using Dirac- δ functions instead of soliton shapes. (c) Similar as (b), for equidistant train 2. of (a).

At a first glance, the spectrum of Fig. 7(b) looks very similar to the typical experimental traces at a single Fourier component, as shown in Fig. 6. This is of course the consequence of the scaling behavior of the spectrum, as the train propagates over distances z [c.f. Eq. (28)]. Consequently, when monitoring a fixed frequency component, the initial high-frequency content will pass by this probe frequency, as the spectrum scales to lower acoustic frequencies.

6. RUBY PHONON SPECTROMETER

The combination of high strains on ultrashort time scales holds promise for exploring THz-coherent electron-phonon interactions in a medium containing two-level centers. Excitation of these local electronic systems using the coherent strain field is a challenging subject, that may extend the analogy between coherent optics and acoustics to the regime of THz phonons. Self-induced transparency has been observed at lower GHz acoustic frequencies in ultrasonic paramagnetic resonance experiments.^{39,40} For THz electron-phonon interactions, however, coherence has up to now not played a significant role, mainly due to the lack of suitable excitation mechanisms for the strain field. Stimulated emission⁴¹ has been well described by incoherent rate equations, and it was only in phonon-induced optical dephasing experiments⁴² that the question of phonon coherence was addressed.

In recent experiments,¹⁷ we have made use of the well-known $\bar{E}(^2E) - 2\bar{A}(^2E)$ crystal-field transition of Cr³⁺-ions embedded in the Al₂O₃ host lattice of a ruby crystal [see Fig. 8(left)]. By exposing this system to trains of ultrashort acoustic solitons, we have demonstrated in Ref [17] coherent, impulsive interactions of the electronic two-level systems for acoustic fields travelling along the crystallographic a axis. Figure 8(right) shows a typical time-resolved R_2 luminescence signal, normalized to the R_1 intensity, obtained in the ruby crystal at a distance of 9 mm from the transducer. The dotted line denotes the signal taken when the excited zone is

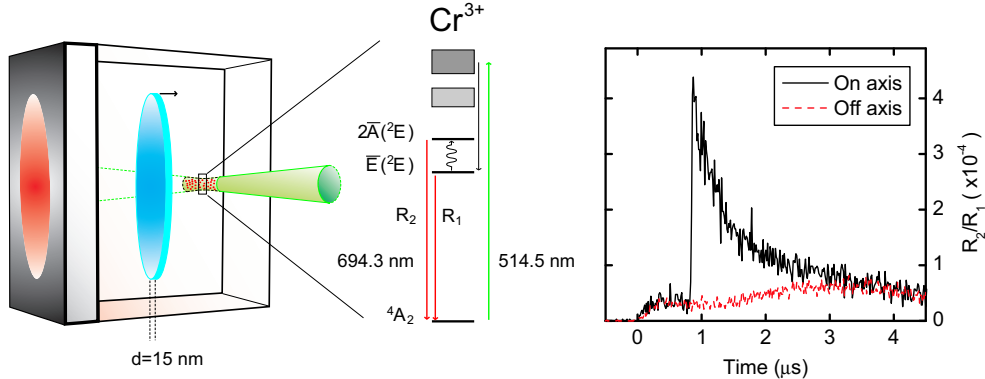


Figure 8. (left) Schematic illustration of detection method using local Cr^{3+} -ions as a probe of 0.87-THz strain components, with level scheme and pumping cycle. (right) Typical on- and off-axis traces of the R_2 -luminescence, normalized to the R_1 intensity, taken at a distance $z = 9$ mm from the transducer. Difference between traces is due to soliton-induced signal.

positioned 1.0 mm below the position of the femtosecond pump laser spot on the transducer. We observe a weak background, which is due to the incoherent heat pulse generated at the position of the transducer. The solid line is the signal when the probe volume is positioned exactly at the height of the excited spot on the metal film. Clearly, an additional contribution is observed that peaks at the arrival time of longitudinal acoustic phonons from the transducer. We have shown¹⁷ that this peak originates from the coherent part of the generated strain, i.e. from the acoustic soliton train.

As the electronic transition has a resonance frequency of 0.87 THz, it can only be excited by a wavepacket with frequency components extending to this high-frequency range. Figure 9(a) shows a typical soliton waveform obtained from our simulations, that is consistent with the Brillouin scattering data. We have analyzed the frequency content in this wavepacket on a local level, by performing short-time Fourier transforms at different parts of the wavepacket, using a square Fourier transformation window of ~ 14 ps. The resulting spectrum as a function of time is shown in Fig. 9(b). The narrow Fourier window limits the spectral resolution to 76 GHz, which is however still small enough to view the typical distribution of spectral components over the wavepacket. We observe that high-frequency, THz frequency components are only present in the first few solitons of the train, and also in a small region of the dispersive tail. Thus, it may well be possible to excite a 0.87-THz two-level medium using this particular wavepacket. New experimental results, extending the pioneering work of Ref. [17], will be presented in the near future.

7. CONCLUSIONS

We have demonstrated several experimental methods to detect the propagation of ultrashort strain wavepackets *in situ* in the bulk of a transparent crystal. Brillouin scattering resolves the development of the wavepacket into a train of ultrashort strain solitons at low temperatures. We find the intricate beating patterns typical for soliton train formation, that are consistent with numerical simulations of the KdV-equation. Further, via the analysis of a train of equidistant solitons we have obtained an analogy between the train spectrum and the orders of a grating. The fine structure between the main grating orders in the spectrum consists of a number of oscillations proportional to the amount of solitons in the train. This method of analysis can be applied reasonably well to the realistic soliton trains in our study, although the periodicity is disturbed by the natural variations in distance between the solitons. The scaling of the soliton train ensures that the orders will shift towards lower frequencies with increasing travelled distance, where they can be detected using Brillouin scattering. Finally, we have briefly described the method of THz coherent electron-phonon interaction in the two-level systems of optically excited ruby. Our results hold promise for the coherent manipulation of ultrashort strain wavepackets, their amplification using inverted two-level systems, and eventually possibly the development of a phonon laser.

This work was supported by the Netherlands Foundation "Fundamenteel Onderzoek der Materie (FOM)" and the "Nederlandse Organisatie voor Wetenschappelijk Onderzoek (NWO)."

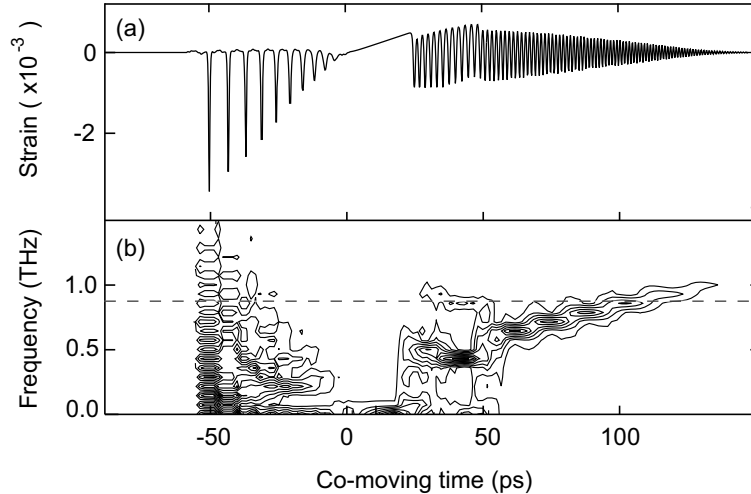


Figure 9. (a) Typical simulated soliton train developed after 0.5 mm of propagation in sapphire. (b) Short-time Fourier transform over of the wavepacket of (a), showing the frequency content at different locations in the wavepacket. Spectral resolution of ~ 76 GHz is determined by the transformation window of 14 ps. (Dash) denotes resonance frequency of the $\bar{E}(^2E) - 2\bar{A}(^2E)$ two-level system in optically excited ruby.

REFERENCES

1. C. Thomsen, H. T. Grahn, H. J. Maris, and J. Tauc, "Surface generation and detection of phonons by picosecond light pulses," *Phys. Rev. B* **34**(6), p. 4129, 1986.
2. T. Guenter *et al.*, "Coherent nonlinear optical response of single quantum dots studied by ultrafast near-field spectroscopy," *Phys. Rev. Lett.* **89**(5), p. 057401, 2002.
3. M. Achermann, U. Siegner, L.-E. Wernersson, and U. Keller, "Ultrafast carrier dynamics around nanoscale schottky contacts studied by femtosecond far- and near-field optics," *Appl. Phys. Lett.* **77**(21), p. 3370, 2000.
4. A. Vertikov, M. Kuball, A. Nurmikko, and H. Maris, "Time-resolved pump-probe experiment with subwavelength lateral resolution," *Appl. Phys. Lett.* **69**, p. 2465, 1996.
5. Y. Sugawara *et al.*, "Watching ripples on crystals," *Phys. Rev. Lett.* **88**, p. 185504, 2002.
6. C. Zhu, J. Tauc, and H. Maris, "Attenuation of longitudinal acoustic phonons in amorphous SiO_2 at frequencies up to 440 GHz," *Phys. Rev. B* **44**, p. 4281, 1991.
7. O. B. Wright and K. Kawashima, "Coherent phonon detection from ultrafast surface vibration," *Phys. Rev. Lett.* **69**(11), p. 1668, 1992.
8. G. Tas and H. J. Maris, "Electron diffusion in metals studied by picosecond ultrasonics," *Phys. Rev. B* **49**, p. 15046, 1994.
9. J. J. Baumberg, D. A. Williams, and K. Köhler, "Ultrafast acoustic phonon ballistics in semiconductor heterostructures," *Phys. Rev. Lett.* **78**(17), p. 3358, 1997.
10. A. Bartels, T. Dekorsy, H. Kurz, and K. Köhler, "Coherent zone-folded longitudinal acoustic phonons in semiconductor superlattices: excitation and detection," *Phys. Rev. Lett.* **82**(5), p. 1044, 1999.
11. Ü. Özgür, C.-W. Lee, and H. O. Everitt, "Control of coherent acoustic phonons in semiconductor quantum wells," *Phys. Rev. Lett.* **86**(24), p. 5604, 2001.
12. A. Kent, N. M. Stanton, L. Challis, and M. Henini, "Generation and propagation of monochromatic acoustic phonons in gallium arsenide," *Appl. Phys. Lett.* **81**(18), p. 3497, 2002.
13. H.-Y. Hao and H. J. Maris, "Dispersion of the long-wavelength phonons in Ge,Si,GaAs, quartz and sapphire," *Phys. Rev. B* **63**(22), p. 4301, 2001.
14. H.-Y. Hao and H. J. Maris, "Study of phonon dispersion in silicon and germanium at long wavelengths using picosecond ultrasonics," *Phys. Rev. Lett.* **84**(24), p. 5556, 2000.
15. H.-Y. Hao and H. J. Maris, "Experiments with acoustic solitons in crystalline solids," *Phys. Rev. B* **64**(6), p. 4302, 2001.

16. O. L. Muskens and J. I. Dijkhuis, "High amplitude, ultrashort, longitudinal strain solitons in sapphire," *Phys. Rev. Lett.* **89**(28), p. 285504, 2002.
17. O. L. Muskens, A. V. Akimov, and J. I. Dijkhuis, "Coherent interactions of terahertz strain solitons and electronic two-level systems in photoexcited ruby," *Phys. Rev. Lett.* , 2004. in press.
18. D. C. Wallace, *Solid State Physics*, vol. 25, p. 301. Academic Press, 1970.
19. C. Kittel, *Introduction to solid state physics*, John Wiley & Sons, 6th ed., 1986.
20. V. I. Karpman, *Non-linear waves in dispersive media*, Pergamon Press, 1st ed., 1975.
21. D. J. Korteweg and G. de Vries, "On the change of form of long waves advancing in a rectangular canal, and on a new type of long stationary waves," *Philos. Mag.* **39**, p. 422, 1895.
22. C. S. Gardner, J. M. Greene, M. D. Kruskal, and R. M. Miura, "Method for solving the korteweg-devries equation," *Phys. Rev. Lett.* **19**(19), p. 1095, 1967.
23. G. B. Whitham, *Linear and Nonlinear Waves*, Wiley, 1 ed., 1974.
24. L. D. Landau and E. M. Lifschitz, *Quantum Mechanics, Non-relativistic Theory*, Pergamon Press, 2nd ed., 1965.
25. B. A. Auld, *Acoustic fields and waves in solids*, vol. 1, Robert E. Krieger Publishing Company, 2nd ed., 1990.
26. E. Infeld, A. Senatorski, and A. A. Skorupski, "Numerical simulations of KP soliton interactions," *Phys. Rev. E* **51**(4), p. 3183, 1995.
27. T. A. Driscoll, "A composite Runge-Kutta method for the spectral solution of semilinear PDE," *J. Comp. Phys.* **182**, p. 357, 2002.
28. A. Balogh and M. Krstic, "Boundary control of the Korteweg - de Vries - Burgers equation: further results on stabilization and numerical demonstration," *IEEE Trans. Autom. Control* **45**, p. 1739, 2000.
29. J. H. Ferziger and M. Perić, *Computational methods for fluid dynamics*, Springer Verlag, 2nd ed., 1999.
30. B. Fornberg and T. A. Driscoll, "A fast spectral algorithm for nonlinear wave equations with linear dispersion," *J. Comp. Phys.* **155**, p. 456, 1999.
31. W. H. Press, S. A. Teukolsky, W. T. Vetterling, and B. P. Flannery, *Numerical Recipes in Fortran 77*. Cambridge University Press, 2nd ed., 1992.
32. T. Saito, O. Matsuda, and O. B. Wright, "Picosecond acoustic phonon pulse generation in nickel and chromium," *Phys. Rev. B* **67**, p. 205421, 2003.
33. O. L. Muskens and J. I. Dijkhuis, "Propagation of ultrashort acoustic wave packets in PbMoO₄ studied by Brillouin spectroscopy," *Physica B* **316-317**, p. 373, 2002.
34. E. P. N. Damen, D. J. Dieleman, A. F. M. Arts, and H. W. de Wijn, "Generation and propagation of coherent phonon beams," *Phys. Rev. B* **64**(17), p. 4303, 2001.
35. E. P. N. Damen, A. F. M. Arts, and H. W. de Wijn, "Experimental verification of Herring's theory of anharmonic phonon relaxation: TeO₂," *Phys. Rev. B* **59**(1), p. 349, 1999.
36. E. P. N. Damen, A. F. M. Arts, and H. W. de Wijn, "High-frequency monochromatic acoustic waves generated by laser-induced thermomodulation," *Phys. Rev. Lett.* **75**(21), p. 4249, 1995.
37. K. H. Hellwege and A. M. Hellwege, eds., *Landolt-Bornstein*, vol. 11, p. 518. Springer, 1979.
38. S. C. Jones, B. A. M. Vaughan, and Y. M. Gupta, "Refractive indices of sapphire under elastic, uniaxial strain compression along the a axis," *J. Appl. Phys.* **90**, p. 4990, 2001.
39. N. S. Shiren, "Self-induced transparency in acoustic paramagnetic resonance," *Phys. Rev. B* **2**(7), p. 2471, 1970.
40. J.-Y. Prieur, J. Joffrin, and K. Lassman, "Acoustic solitons, phonon echoes and sound amplification in Si:B at very low temperatures," *Physica B* **316-317**, p. 125, 2002.
41. P. Hu, "Stimulated emission of 29-cm⁻¹ phonons in ruby," *Phys. Rev. Lett.* **44**(6), p. 417, 1980.
42. M. H. F. Overwijk, J. I. Dijkhuis, and H. W. de Wijn, "Superfluorescence and amplified spontaneous emission of 29-cm⁻¹ phonons in ruby," *Phys. Rev. Lett.* **65**(16), p. 2015, 1990.